# Finite Element Analysis of MHD Flow of Micropolar Fluid over a Shrinking Sheet with a Convective Surface Boundary Condition

**D. Gupta[1], L. Kumar[1]\*, O. Anwar Bég[2], and B. Singh[1]**

[1]*Department of Mathematics, Jaypee Institute of Information Technology, A-10, Sector-62, Noida-201307, Uttar Pradesh, India*

[2]*Gort Engovation (Biomechanics and Aerospace), Southmere av. 15, Bradford, BD73NU England, UK*

Received October 26, 2017

**Abstract**—This paper presents a numerical solution for the steady mixed convection magneto-hydrodynamic (MHD) flow of an electrically conducting micropolar fluid over a porous shrinking sheet. The velocity of shrinking sheet and magnetic field are assumed to vary as power functions of the distance from the origin. A convective boundary condition is used rather than the customary conditions for temperature, i.e., constant surface temperature or constant heat flux. With the aid of similarity transformations, the governing partial differential equations are transformed into a system of nonlinear ordinary differential equations, which are solved numerically, using the variational finite element method (FEM). The influence of various emerging thermophysical parameters, namely suction parameter, convective heat transfer parameter, magnetic parameter and power index on velocity, microrotation and temperature functions is studied extensively and is shown graphically. Additionally the skin friction and rate of heat transfer, which provide an estimate of the surface shear stress and the rate of cooling of the surface, respectively, have also been computed for these parameters. Under the limiting case an analytical solution of the flow velocity is compared with the present numerical results. An excellent agreement between the two sets of solutions is observed. Also, in order to check the convergence of numerical solution, the calculations are carried out by reducing the mesh size. The present study finds applications in materials processing and demonstrates excellent stability and convergence characteristics for the variational FEM code.

## 1. INTRODUCTION

The boundary layer flow induced by stretching surface is an important type of flow occurring in several materials manufacturing and chemical flow processes. These include wire drawing, paper production, glass-fiber production, liquid metal and polymer sheet synthesis. In all these cases, the mechanical properties of the final product are significantly affected by the rate of cooling and stretching in the process and material characteristics may, therefore, be manipulated to desired specifications. The pioneering work in this area was carried out by Sakiadis [1]. Tsou et al. [2] carried out combined analytical and experimental study of the flow and heat transfer in the boundary layer on a continuous moving surface. Boundary layer flow of a Newtonian fluid caused by a linearly stretching sheet was described by Crane [3], who derived an exact similarity solution in closed analytical form. Thereafter, various aspects of Newtonian fluid flows from a stretching surface have been reported by Grubka and Bobba [4], Elbashbeshy [5], Magyari and Keller [6], Andersson [7] and Cortell [8]. However, many engineering processes utilize non-Newtonian fluids such as paints, lubricants, human and animal blood, body fluids, polymers, colloidal fluids and suspension fluids. The classical theories of continuum mechanics cannot be used for the realistic description of the flow of these fluids. Eringen [9] has formulated the theory of micropolar fluids, which describes the physics of such fluids by taking into account the effect arising

---

*E-mail: lokendma@gmail.com

from local structure and micro-motions of the fluid elements. Micropolar fluids can support couple stresses, shear stresses and body couples and also exhibit micro-rotational effects and inertia. The fundamentals of micropolar fluid theory, with some simple engineering applications, are elucidated in the book by Eringen [10]. More advanced scenarios of a multi-physical nature are covered in the monograph by Bég et al. [11]. Eringen [12] has extended the theory of microfluids (or "micromorphic" fluids) to thermomicrofluids, of which thermo-micropolar fluids are again a special case. This theory takes into account thermal effects, i.e., heat conduction, convection and dissipation. These effects were not included in the classical field theories.

Boundary layer flow from a shrinking sheet is also a significant problem in modern materials processing technologies. This type of flow was first examined analytically by Wang [13]. Later, Miklavcic and Wang [14] presented closed-form solutions for the Navier−Stokes equations for the flow over a shrinking sheet. Shrinking sheet flow is essentially a backward flow as discussed by Goldstein [15]. From the physical point of view, steady flow over a shrinking sheet is not possible since the generated vorticity is not confined within the boundary layer. To overcome this difficulty, the flow requires a certain amount of external opposite force at the sheet. This has been extensively discussed in the literature. Some relevant expositions in this regard are Miklavcic and Wang [14], Wang [16], and Bachok et al. [17]. Fang et al. [18] computed solutions for the unsteady flow over a shrinking surface with mass suction and highlighted the deviation in flow behavior for an unsteady shrinking sheet compared with an unsteady stretching sheet. Flow and heat transfer of a viscous fluid over a stretching/shrinking sheet was later considered by Fang et al. [19]. Numerical solutions for the boundary layer flow and heat transfer over a porous shrinking sheet in the presence of thermal radiation flux were obtained by Bhattacharyya and Layek [20]. The shrinking sheet problem was extended to micropolar fluids by Ishak et al. [21] who considered stagnation point flow. Yacob and Ishak [22] subsequently obtained computational solutions for coupled flow and heat transfer over a shrinking sheet immersed in a micropolar fluid.

In the above-mentioned studies, the effect of magnetic field on the flow and heat transfer has not been considered. Magnetohydrodynamics (MHD) with heat transfer from a shrinking sheet is important in many manufacturing processes in the industry. Keeping in view some specific applications such as polymer processing technology, many investigators have analyzed the effect of magnetic field on momentum and thermal boundary layer flow characteristics. Muhaimin et al. [23] conducted numerical computations to examine the effects of heat and mass transfer on nonlinear MHD flow over a shrinking sheet with wall suction/injection. Magnetohydrodynamic flow of a viscous fluid over a shrinking sheet was examined by Fang and Zhang [24]. They obtained the closed-form exact solution of the Navier−Stokes equations. Using the homotopy semi-numerical technique, Nadeem and Hussain [25] investigated the magnetohydrodynamic flow of a viscous fluid over a nonlinear porous shrinking sheet. Schit and Haldar [26] reported on the combined effects of radiation and magnetic field on the flow and heat transfer over a shrinking sheet by taking into account the power function variation of magnetic field and shrinking velocity from the origin. Hayat et al. [27] studied the magnetohydrodynamic dissipative stagnation point flow of micropolar fluid over a shrinking surface with heat source/sink effects. A computational study of MHD stagnation point flow of a micropolar fluid towards a heated shrinking sheet was conducted by Ashraf and Bashir [28] using a finite-difference algorithm. Das [29] investigated the slip effects on MHD mixed convection flow of a micropolar fluid towards a shrinking vertical sheet.

Heat transfer with convective boundary condition is more general and realistic especially with respect to various engineering and industrial processes including material drying [30], laser pulse heating [31] and transpiration cooling [32]. Aziz [33] examined the Blasius flow of a viscous fluid with convective boundary condition and demonstrated the condition for the similarity solution to exist. Boundary layer flow and heat transfer of a viscous fluid over a permeable surface with a convective boundary condition was presented by Ishak [34]. Numerical solution of MHD mixed convection from a vertical plate with heat and mass transfer and a convective boundary condition at the plate was carried out by Makinde and Aziz [35]. Yao et al. [36] studied the heat transfer of a viscous fluid over a stretching/shrinking sheet with a convective boundary condition. They showed that convective boundary condition results in temperature slip at the wall and is affected by mass transfer parameter. Using an implicit finite difference scheme in combination with the quasi-linearization technique Subhashini et al. [37] reported on the double-diffusive convection from a vertical permeable flat surface under a convective boundary condition. Magneto-convective boundary layer flow from a translating vertical plate with convective heat exchange at the surface with cross diffusion effects was studied by Makinde et al. [38] using MAPLE.

204 GUPTA et al.

Recently Yacob and Ishak [39] investigated the stagnation point flow of a micropolar fluid towards a stretching/shrinking sheet with a convective surface boundary condition and showed that heat transfer rate at the surface for the stretching case exceeds that for the shrinking case.

The aim of the present paper is to analyze the effect of magnetic field on mixed convection flow and heat transfer of magneto-micropolar fluid over a permeable shrinking sheet. The shrinking velocity and the magnetic field are assumed to vary as power functions of distance from the origin. The governing nonlinear partial differential equations are rendered into a coupled, highly nonlinear system of nonlinear ordinary differential equations by applying a suitable similarity transformation. The resulting normalized two-point boundary value problem, under appropriate boundary conditions, is solved numerically by using a variational formulation of the finite element method (FEM). The influence of the pertinent dimensionless parameters on the velocity, microrotation and temperature functions has been depicted graphically. The numerical results for the skin friction coefficient and the local Nusselt number have also been computed. In order to check the convergence of the numerical solution, calculations are carried out by reducing the mesh size. The FEM code is also validated with previous studies demonstrating excellent correlation. The current study is relevant to thermophysical sheet processing of electro-conductive polymers [40, 41] and aims to further reveal the influence of MHD effects on micro-structural and thermofluid characteristics in such systems.

## 2. MATHEMATICAL MODEL

Let us consider a steady laminar boundary layer flow of an incompressible electrically conducting micropolar fluid over a porous shrinking sheet. The $x$ axis is taken along the sheet and $y$ axis is taken normal to it. The continuous shrinking sheet is assumed to move with a velocity according to power-law form, i.e., $U(x) = -ax^n$, where $a > 0$ is constant of proportionality and $n$ is a power index. A magnetic field $B(x)$ is applied perpendicular to the surface of the sheet. The strength of the magnetic field is $B(x) = B_0 x^{\frac{n-1}{2}}$, where $B_0$ represents the constant magnetic field strength applied perpendicular to the shrinking sheet. The special form of the magnetic field $B(x)$ is chosen to obtain a similarity solution. This form has also been considered by Chiam [42]. Since the magnetic Reynolds number is small for most of the fluids in industrial applications, we assume that the induced magnetic field is negligible. It is also assumed that there is no applied electric field and the electric field due to polarization of charges is negligible. Moreover, the viscous dissipation effect is neglected in the present study. The flow configuration and the coordinate system are shown in the Fig. 1. Under the above assumptions along with the boundary layer approximations, the equations that govern the problem under consideration can be expressed as follows:

*Conservation of mass*:

$$\frac{\partial u}{\partial x} + \frac{\partial v}{\partial y} = 0, \tag{1}$$

*Conservation of linear momentum*:

$$u\frac{\partial u}{\partial x} + v\frac{\partial u}{\partial y} = \left(\frac{\mu + S}{\rho}\right)\frac{\partial^2 u}{\partial y^2} + \frac{S}{\rho}\frac{\partial N}{\partial y} + g_e\beta(T - T_\infty) - \frac{\sigma_0 B^2(x)}{\rho}u, \tag{2}$$

*Conservation of angular momentum*:

$$u\frac{\partial N}{\partial x} + v\frac{\partial N}{\partial y} = \frac{\gamma}{\rho j}\frac{\partial^2 N}{\partial y^2} - \frac{S}{\rho j}\left(2N + \frac{\partial u}{\partial y}\right), \tag{3}$$

*Conservation of energy*:

$$u\frac{\partial T}{\partial x} + v\frac{\partial T}{\partial y} = \frac{\kappa}{\rho c_p}\frac{\partial^2 T}{\partial y^2}, \tag{4}$$
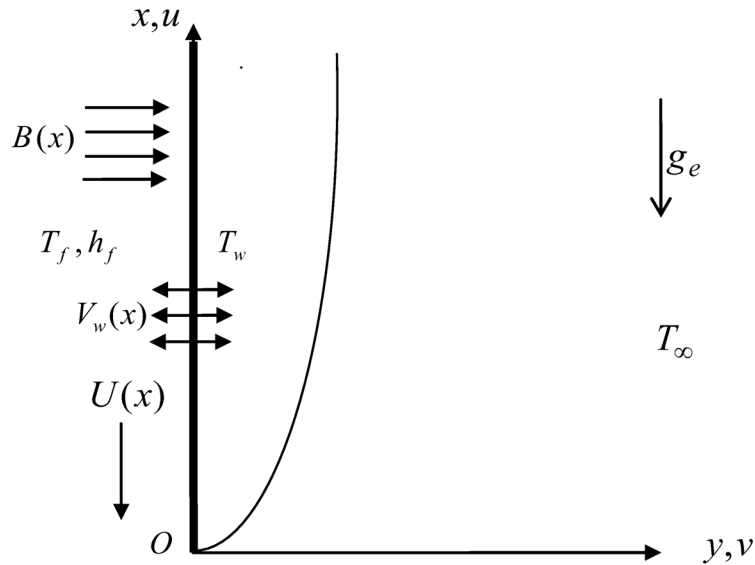
**Fig. 1.** Physical model and coordinate system.

where the spin gradient viscosity $\gamma$ is given by $\gamma = \left(\mu + \frac{S}{2}\right) j$ and $j = (\nu/a)\, x^{1-n}$.

The boundary conditions for the flow field are given by

$$u = U(x) = -ax^n, \quad v = V_w x^{\frac{n-1}{2}}, \quad N = -0.5\frac{\partial u}{\partial y} \quad \text{at} \ = 0,$$

$$u \to 0, \quad N \to 0, \quad \text{as} \ y \to \infty. \tag{5}$$

On the other hand, it is assumed that the left side of the sheet surface is heated by convection from a hot fluid of uniform temperature $T_f$, which provides a heat transfer coefficient $h_f$. The temperature boundary conditions at the surface of the sheet and far into the cold fluid are given as

$$-\kappa\frac{\partial T}{\partial y} = h_f \left(T_f - T_w\right) \quad \text{at} \ y = 0,$$

$$T \to T_\infty \quad \text{as} \ y \to \infty, \tag{6}$$

where $T_f > T_w > T_\infty$.

In order to solve Eqs. (1)–(4), we introduce the following similarity transformations:

$$\eta = \sqrt{\frac{a\,(n+1)\,x^{n-1}}{2\nu}}\,y, \quad \phi = \sqrt{\frac{2a\nu x^{n+1}}{(n+1)}}\,f, \quad N = \sqrt{\frac{a^3\,(n+1)\,x^{3n-1}}{2\nu}}\,g, \quad \theta = \frac{T - T_\infty}{T_f - T_\infty}, \tag{7}$$

where stream function $\phi$, satisfies the continuity equation (1) automatically with $u = \partial\phi/\partial y$ and $v = -\partial\phi/\partial x$. Using (7) we obtain

$$u = ax^n f', \quad v = -x^{\frac{n-1}{2}}\sqrt{\frac{a\nu\,(n+1)}{2}}\left[f\,(\eta) + \left(\frac{n-1}{n+1}\right)\eta f'\,(\eta)\right]. \tag{8}$$

Using (7) and (8), Eqs. (2)–(4) reduce to

$$(1 + K)f''' + ff'' - \frac{2n}{(n+1)}\left(f'\right)^2 - \frac{2}{(n+1)}Mf' + Kg' + \frac{2}{(n+1)}\sigma\theta = 0, \tag{9}$$

$$\left(1 + \frac{K}{2}\right)g'' + fg' - \left(\frac{3n-1}{n+1}\right)f'g - \frac{2}{(n+1)}K\left(2g + f''\right) = 0, \tag{10}$$

$$\theta'' + \Pr f\theta' = 0, \tag{11}$$

and the transformed boundary conditions (5) and (6) take the form

$$f = -\lambda, \ \ f' = -1, \ \ g = -0.5f'', \ \ \theta' = -c\left[1 - \theta\left(0\right)\right] \ \ \text{at} \ \eta = 0, \tag{12}$$

$$f' = 0, \ \ g = 0, \ \ \theta = 0 \ \ \text{as} \ \eta \to \infty, \tag{13}$$

where primes denote differentiation with respect to $\eta$ only, $K = S/\mu$ (the coupling constant parameter), $M = \sigma_0 B_0^2/\rho a$ (the magnetic parameter), $\sigma = Gr_x/\text{Re}_x^2$ (buoyancy parameter), $Gr_x = g_e\beta(T_w - T_\infty)x^3/\nu^2$ (local Grashof number), $\text{Re}_x = ax^{n+1}/\nu$ (local Reynolds number), $\Pr = \mu c_p/\kappa$ (Prandtl number), $\lambda = \sqrt{2}V_w \big/ \left(\sqrt{\nu a(n+1)}\right)$ (suction parameter); $\lambda > 0$ corresponds to suction and $\lambda < 0$ corresponds to injection (is not considered in the present study), $c = \left(h_f\sqrt{2\nu x^{(1-n)}}\right)\big/\left(\kappa\sqrt{a\left(n+1\right)}\right)$ (convective heat transfer parameter). It may be noted that the heat transfer coefficient $h_f$ should be proportional to $x^{-(1-n)/2}$ so as to eliminate the dependence of $c$ on $x$, i.e., $h_f = ex^{-(1-n)/2}$, where $e$ is a constant.

The quantities of physical interest in this problem are the local skin friction coefficient and the local Nusselt number, which are, respectively, defined as

$$C_f = \frac{2\tau_w}{\rho U^2}, \quad Nu_x = \frac{qx}{\kappa(T_f - T_\infty)}, \tag{14}$$

where the local wall shear stress $\tau_w$ and the heat transfer from the plate $q$ are given by

$$\tau_w = -\left[(\mu + S)\frac{\partial u}{\partial y} + SN\right]_{y=0}, \quad q = -\kappa\left(\frac{\partial T}{\partial y}\right)_{y=0}. \tag{15}$$

Using the similarity transformations given in (7), we obtain

$$C_f\left(\text{Re}_x\right)^{1/2} = -\sqrt{\frac{(n+1)}{2}}\left(2 + K\right)f''\left(0\right) \ \ \text{and} \ \ \frac{Nu_x}{\sqrt{\text{Re}_x}} = -\sqrt{\frac{(n+1)}{2}}\theta'\left(0\right). \tag{16}$$

## 3. FINITE ELEMENT METHOD (FEM) SOLUTION

The finite element method has been implemented to obtain the numerical solution of the system of nonlinear ordinary differential equations (9)–(11) subject to boundary conditions (12)–(13). This method is extremely efficient and has been applied to study different problems in fluid mechanics, heat transfer, chemical processing, solid mechanics, and other fields also. The general details of the finite element method can be found in Reddy [43]. Further recent studies using the variational FEM approach include Gupta et al. [44, 45], Rana et al. [46], Kumar [47], and Bég et al. [48].

In order to apply the finite element method first we assume

$$f' = h. \tag{17}$$

Then Eqs. (9)–(11) take the form

$$(1 + K)h'' + fh' - \frac{2n}{(n+1)}h^2 - \frac{2}{(n+1)}Mh + Kg' + \frac{2}{(n+1)}\sigma\theta = 0, \tag{18}$$

$$(1 + \frac{K}{2})g'' + fg' - \left(\frac{3n-1}{n+1}\right)hg - \frac{2K}{(n+1)}\left(2g + h'\right) = 0, \tag{19}$$

$$\theta'' + \Pr f\theta' = 0, \tag{20}$$

and the corresponding boundary conditions now become

$$f = -\lambda, \quad h = -1, \quad g = -0.5h', \quad \theta' = -c\left[1 - \theta\left(0\right)\right] \quad \text{at} \quad \eta = 0, \tag{21}$$

$$h \to 0, \quad g \to 0, \quad \theta \to 0 \quad \text{as} \quad \eta \to \infty. \tag{22}$$

For the computational purposes, infinity has been fixed at 8. It is observed that the value greater than 8 does not result in any significant change in the numerical results.

### 3.1. Variational Formulation

The variational form associated with Eqs. (17)–(20) over a typical two-noded element $(\eta_e, \eta_{e+1})$ is given by

$$\int_{\eta_e}^{\eta_{e+1}} w_1 \left\{f' - h\right\} d\eta = 0, \tag{23}$$

$$\int_{\eta_e}^{\eta_{e+1}} w_2 \left\{(1 + K)h'' + fh' - \frac{2n}{(n+1)}h^2 - \frac{2}{(n+1)}Mh + Kg' + \frac{2}{(n+1)}\sigma\theta\right\} d\eta = 0, \tag{24}$$

$$\int_{\eta_e}^{\eta_{e+1}} w_3 \left\{(1 + \frac{K}{2})g'' + fg' - \left(\frac{3n-1}{n+1}\right)hg - \frac{2K}{(n+1)}\left(2g + h'\right)\right\} d\eta = 0, \tag{25}$$

$$\int_{\eta_e}^{\eta_{e+1}} w_4 \left\{\theta'' + \Pr f\theta'\right\} d\eta = 0, \tag{26}$$

where $w_1$, $w_2$, $w_3$, and $w_4$ are weight functions, which may be viewed as the variation in $f$, $h$, $g$, and $\theta$, respectively.

### 3.2. Finite Element Formulation

The finite element model may be obtained from Eqs. (23)–(26) by substituting finite element approximation of the form

$$f = \sum_{j=1}^{2} f_j \psi_j, \quad h = \sum_{j=1}^{2} h_j \psi_j, \quad g = \sum_{j=1}^{2} g_j \psi_j, \quad \theta = \sum_{j=1}^{2} \theta_j \psi_j, \tag{27}$$

with $w_1 = w_2 = w_3 = w_4 = \psi_i$ $(i = 1, 2)$, where the shape functions $\psi_i$ for a typical line element $(\eta_e, \eta_{e+1})$ are given by:

$$\psi_1 = \frac{\eta_{e+1} - \eta}{\eta_{e+1} - \eta_e}, \quad \psi_2 = \frac{\eta - \eta_e}{\eta_{e+1} - \eta_e}, \quad \eta_e \leq \eta \leq \eta_{e+1}. \tag{28}$$

The finite element equations are, therefore, given by

$$\begin{bmatrix} [K^{11}][K^{12}][K^{13}][K^{14}] \\ [K^{21}][K^{22}][K^{23}][K^{24}] \\ [K^{31}][K^{32}][K^{33}][K^{34}] \\ [K^{41}][K^{42}][K^{43}][K^{44}] \end{bmatrix} \begin{bmatrix} \{f\} \\ \{h\} \\ \{g\} \\ \{\theta\} \end{bmatrix} = \begin{bmatrix} \{b^1\} \\ \{b^2\} \\ \{b^3\} \\ \{b^4\} \end{bmatrix}, \tag{29}$$

$[K^{mn}]$ and $[b^m]$ $(m, n = 1, 2, 3, 4)$ are the matrices of order $2 \times 2$ and $2 \times 1$, respectively, and are given by

$$K_{ij}^{11} = \int_{\eta_e}^{\eta_{e+1}} \psi_i \frac{d\psi_j}{d\eta} d\eta, K_{ij}^{12} = -\int_{\eta_e}^{\eta_{e+1}} \psi_i \psi_j d\eta, \quad K_{ij}^{13} = K_{ij}^{14} = 0, \quad K_{ij}^{21} = 0,$$

$$K_{ij}^{22} = -(1+K) \int_{\eta_e}^{\eta_{e+1}} \frac{d\psi_i}{d\eta} \frac{d\psi_j}{d\eta} d\eta + \int_{\eta_e}^{\eta_{e+1}} \bar{f} \psi_i \frac{d\psi_j}{d\eta} d\eta - \frac{2n}{(n+1)} \int_{\eta_e}^{\eta_{e+1}} \bar{h} \psi_i \psi_j d\eta - \frac{2M}{(n+1)} \int_{\eta_e}^{\eta_{e+1}} \psi_i \psi_j d\eta,$$

$$K_{ij}^{23} = K \int_{\eta_e}^{\eta_{e+1}} \psi_i \frac{d\psi_j}{d\eta} d\eta, \quad K_{ij}^{24} = \frac{2\sigma}{(n+1)} \int_{\eta_e}^{\eta_{e+1}} \psi_i \psi_j d\eta, \quad K_{ij}^{31} = 0, \quad K_{ij}^{32} = -\frac{2K}{(n+1)} \int_{\eta_e}^{\eta_{e+1}} \psi_i \frac{d\psi_j}{d\eta} d\eta,$$

$$K_{ij}^{33} = -\left(1 + \frac{K}{2}\right) \int_{\eta_e}^{\eta_{e+1}} \frac{d\psi_i}{d\eta} \frac{d\psi_j}{d\eta} d\eta + \int_{\eta_e}^{\eta_{e+1}} \bar{f} \psi_i \frac{d\psi_j}{d\eta} d\eta - \left(\frac{3n-1}{n+1}\right) \int_{\eta_e}^{\eta_{e+1}} \bar{h} \psi_i \psi_j d\eta$$

$$- \frac{4K}{(n+1)} \int_{\eta_e}^{\eta_{e+1}} \psi_i \psi_j d\eta,$$

$$K_{ij}^{34} = 0, \quad K_{ij}^{41} = K_{ij}^{42} = K_{ij}^{43} = 0, \quad K_{ij}^{44} = -\int_{\eta_e}^{\eta_{e+1}} \frac{d\psi_i}{d\eta} \frac{d\psi_j}{d\eta} d\eta + \mathrm{Pr} \int_{\eta_e}^{\eta_{e+1}} \bar{f} \psi_i \frac{d\psi_j}{d\eta} d\eta, \tag{30}$$

and

$$b_i^1 = 0, \quad b_i^2 = -(1+K)\left(\psi_i \frac{dh}{d\eta}\right)_{\eta_e}^{\eta_{e+1}},$$

$$b_i^3 = -\left(1 + \frac{K}{2}\right)\left(\psi_i \frac{dg}{d\eta}\right)_{\eta_e}^{\eta_{e+1}}, \quad b_i^4 = -\left(\psi_i \frac{d\theta}{d\eta}\right)_{\eta_e}^{\eta_{e+1}}, \tag{31}$$

where $\bar{f} = \sum\limits_{i=1}^{2} \bar{f}_i \psi_i$ and $\bar{h} = \sum\limits_{i=1}^{2} \bar{h}_i \psi_i$ are assumed to be known.

The resulting system of equations obtained after the assembly of element equations is nonlinear. Therefore, an iterative scheme is used for solving it. The system is linearized by incorporating the function $\bar{f}$ and $\bar{h}$ known at a lower iteration level. Computations for the functions $f$, $g$, $h$, and $\theta$ are then carried out for a higher level. This process is repeated till the desired accuracy of 0.00005 is obtained. In order to check the convergence of the results, calculations are carried out for increasing number of elements, as shown in Table 1. It is clear from the table that as the number of elements increases beyond 160, no significant variation in the values of $f$, $g$, and $\theta$ is observed. Thus, the final results are reported for 160 elements in all other tables. Mesh independence is therefore clearly demonstrated.

When the buoyancy force is absent ($\sigma = 0$), the fluid is Newtonian ($K = 0$) and the sheet is shrinking linearly ($n = 1$), the exact solution for $f(\eta)$, as obtained by Fang and Zhang[24], is given by

$$f(\eta) = \lambda - \left(1 - e^{-\eta z}\right)/z, \tag{32}$$

where $z = 0.5[\lambda + (\lambda^2 + 4M - 4)^{1/2}]$.

Table 2 shows the comparison of the flow velocity $f'(\eta)$ obtained by us using finite element method and the above by analytical method. Inspection of the table shows that numerical results obtained are in complete agreement with each other confirming the validity and accuracy of the FEM. Confidence in the present variational FEM code is therefore high.

**Table 1.** Convergence of results with the variation of number of elements ($K = 1$, $\mathrm{Pr} = 0.733$, $\sigma = 5$, $\lambda = 3.5$, $c = 1$, $M = 3$, $n = 0.5$)

| Number of elements | $f(0.8)$ | $g(0.8)$ | $\theta(0.8)$ |
|---|---|---|---|
| 20 | 3.2516 | $-0.1712$ | 0.0355 |
| 40 | 3.2427 | $-0.2084$ | 0.0411 |
| 60 | 3.2416 | $-0.2181$ | 0.0421 |
| 80 | 3.2414 | $-0.2220$ | 0.0424 |
| 100 | 3.2413 | $-0.2240$ | 0.0426 |
| 120 | 3.2413 | $-0.2251$ | 0.0427 |
| 140 | 3.2413 | $-0.2258$ | 0.0427 |
| 160 | 3.2413 | $-0.2263$ | 0.0427 |
| 180 | 3.2413 | $-0.2263$ | 0.0428 |
| 200 | 3.2413 | $-0.2263$ | 0.0428 |

**Table 2.** Comparison of the flow velocity $f'(\eta)$ obtained by analytical method (Ref. [24]) and FEM (this paper) ($K = 0$, $\mathrm{Pr} = 0.733$, $\sigma = 0$, $\lambda = 3$, $c = 1$, $M = 1$, $n = 1$) in the special case

| $\eta$ | $f'(\eta)$ | |
|---|---|---|
| | Ref. [24] | FEM (ours) |
| 0 | $-1$ | $-1$ |
| 1 | $-0.04979$ | $-0.04915$ |
| 2 | $-0.00248$ | $-0.00243$ |
| 3 | $-0.00012$ | $-0.00012$ |
| 4 | $-0.00001$ | $-0.00001$ |
| 5, 6, 7, 8 | $0.00000$ | $0.00000$ |

**Table 3.** The skin friction coefficient $f''(0)$ for different values of $\lambda$, $c$, $M$, and $n$ ($K = 1$, $\mathrm{Pr} = 0.733$, $\sigma = 5$)

| $c = 1$, $M = 3$, $n = 0.5$ | | $\lambda = 3.5$, $M = 3$, $n = 0.5$ | | $\lambda = 3.5$, $c = 1$, $n = 0.5$ | | $\lambda = 3.5$, $c = 1$, $M = 3$ | |
|---|---|---|---|---|---|---|---|
| $\lambda$ | $f''(0)$ | $c$ | $f''(0)$ | $M$ | $f''(0)$ | $n$ | $f''(0)$ |
| 2.0 | 2.98754 | 0.25 | 3.10723 | 0 | 2.67811 | 0.5 | 3.36981 |
| 2.5 | 3.06345 | 0.5 | 3.21020 | 1 | 2.95198 | 1 | 3.09404 |
| 3.0 | 3.19543 | 1.0 | 3.36981 | 3 | 3.36981 | 2 | 2.77977 |
| 3.5 | 3.36981 | 1.5 | 3.48795 | 6 | 3.85042 | 3 | 2.60160 |
| 4.0 | 3.57500 | 2.0 | 3.57900 | 9 | 4.24196 | 5 | 2.40258 |

**Table 4.** The heat transfer rate $-\theta'(0)$ for different values of $\lambda$, $c$, $M$, and $n$ ($K = 1$, $\mathrm{Pr} = 0.733$, $\sigma = 5$)

| $c = 1$, $M = 3$, $n = 0.5$ | | $\lambda = 3.5$, $M = 3$, $n = 0.5$ | | $\lambda = 3.5$, $c = 1$, $n = 0.5$ | | $\lambda = 3.5$, $c = 1$, $M = 3$ | |
|---|---|---|---|---|---|---|---|
| $\lambda$ | $-\theta'(0)$ | $c$ | $-\theta'(0)$ | $M$ | $-\theta'(0)$ | $n$ | $-\theta'(0)$ |
| 2.0 | 0.56947 | 0.25 | 0.22581 | 0 | 0.70508 | 0.5 | 0.70680 |
| 2.5 | 0.62728 | 0.5 | 0.41326 | 1 | 0.70583 | 1 | 0.70617 |
| 3.0 | 0.67192 | 1.0 | 0.70680 | 3 | 0.70680 | 2 | 0.70538 |
| 3.5 | 0.70680 | 1.5 | 0.92634 | 6 | 0.70771 | 3 | 0.70489 |
| 4.0 | 0.73453 | 2.0 | 1.09686 | 9 | 0.70833 | 5 | 0.70429 |

## 4. RESULTS AND DISCUSSION

Numerical computations have been performed for velocity, microrotation and temperature functions for various values of important physical parameters such as suction parameter $\lambda$, convective heat transfer parameter $c$, magnetic parameter $M$, and power index $n$. The micropolar coupling constant parameter $K$, buoyancy parameter $\sigma$ and Prandtl number $\mathrm{Pr}$ are kept fixed at 1, 5, and 0.733 respectively. These results are shown graphically in Figs. 2–13. The skin friction coefficient and local Nusselt number have also been computed for these parameters and are tabulated in Tables 3 and 4. Higher values of suction parameter are taken so as to sustain steady flow near the sheet by confining the generated vorticity inside the boundary layer.

The influence of the suction parameter $\lambda$ on the velocity is examined in Fig. 2. Velocity decreases with increase in suction parameter. Negative values of the velocity near the sheet indicate that the flow
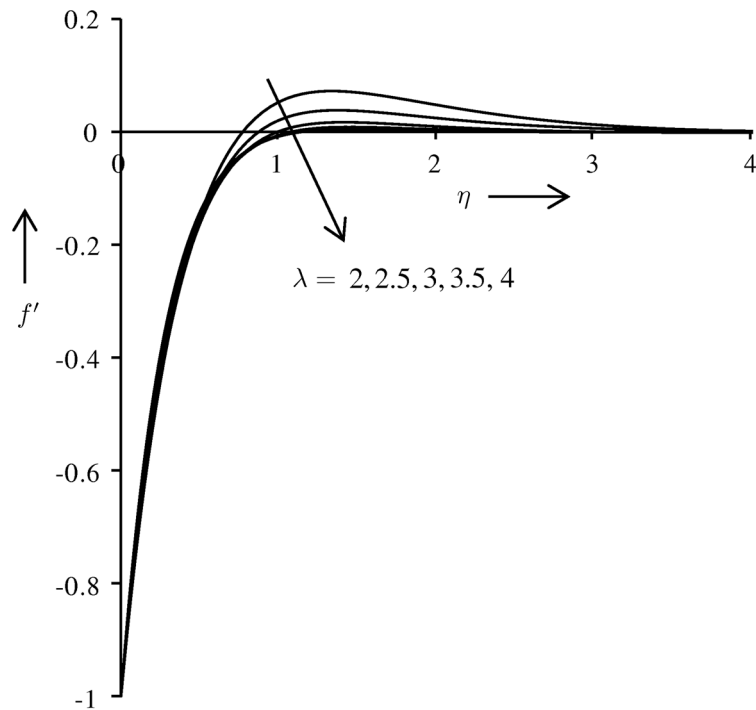
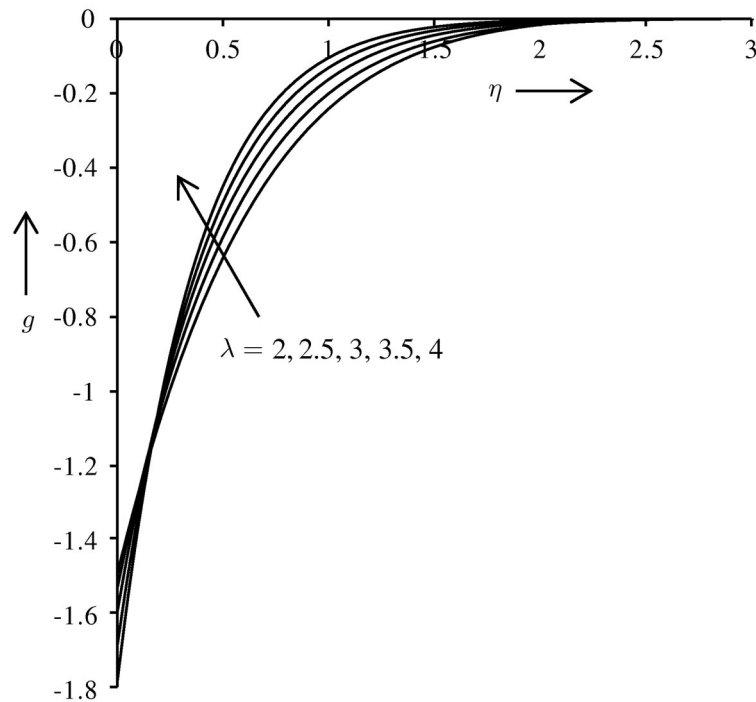**Fig. 2.** Velocity distribution for different $\lambda$ ($c = 1$, $M = 3$, $n = 0.5$).



**Fig. 3.** Microrotation distribution for different $\lambda$ ($c = 1$, $M = 3$, $n = 0.5$).

reversal is induced by the suction. Figure 3 shows the effect of $\lambda$ on the microrotation. In the vicinity of the sheet microrotation decreases with increase in the suction parameter $\lambda$; after covering a small distance from the sheet the converse behavior is observed. Negative values of microrotation indicate the reverse gyratory motions (spin) of micro-elements. The effect of suction parameter $\lambda$ on the temperature is presented in Fig. 4. It is clear from the figure that the temperature decreases as suction increases and, consequently, the thermal boundary layer thickness decreases. A similar observation has been
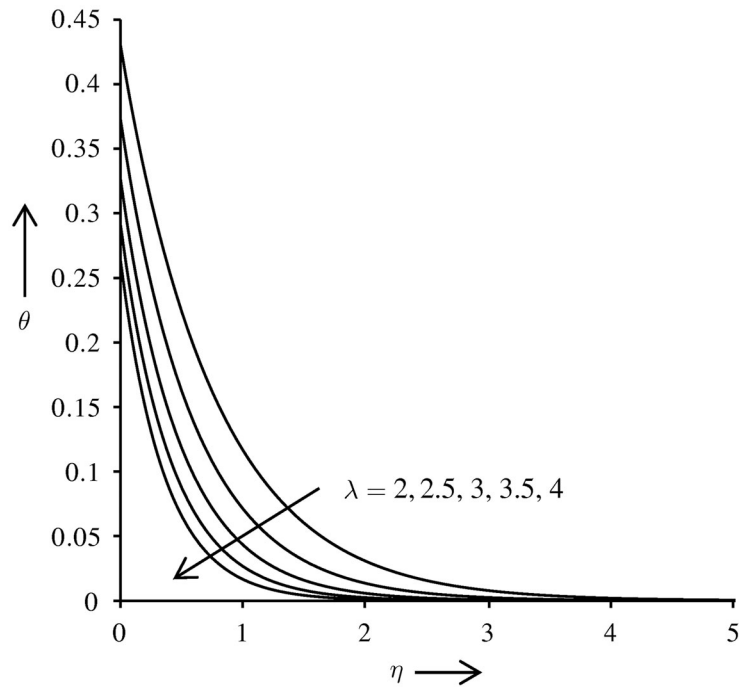
**Fig. 4.** Temperature distribution for different $\lambda$ ($c = 1$, $M = 3$, $n = 0.5$).
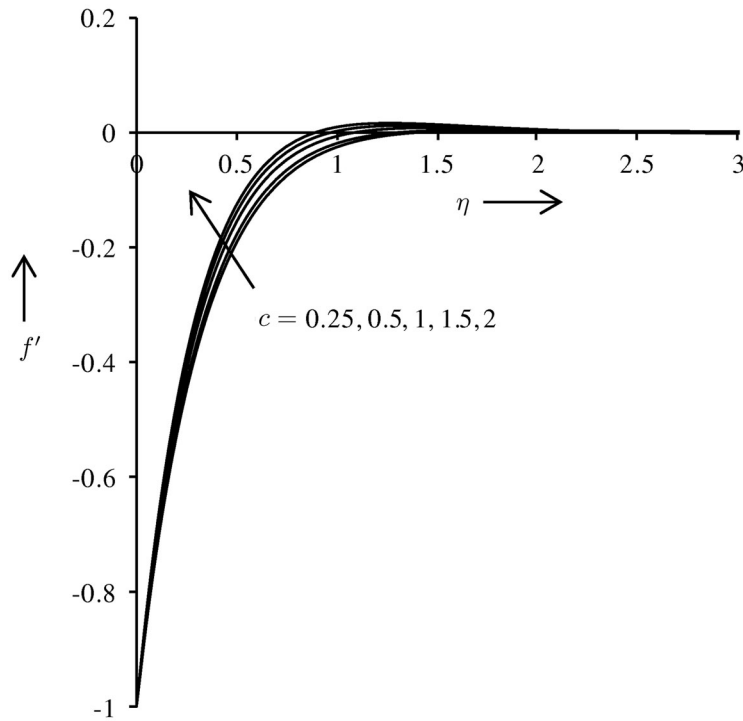


**Fig. 5.** Velocity distribution for different $c$ ($\lambda = 3.5$, $M = 3$, $n = 0.5$).

reported by Bhattacharyya and Layek [20] and Muhaimin et al. [23]. Thus, suction parameter can be used effectively for controlling both the flow and heat transfer characteristics.

Figure 5 illustrates the velocity distribution for different values of convective parameter, $c$. It is apparent that velocity increases with rising convective parameter. As the convective parameter increases, boundary layer thickness therefore decreases. The velocity profile is found to be in qualitative agreement with those obtained by Makinde and Aziz [35]. The influence of the convective parameter
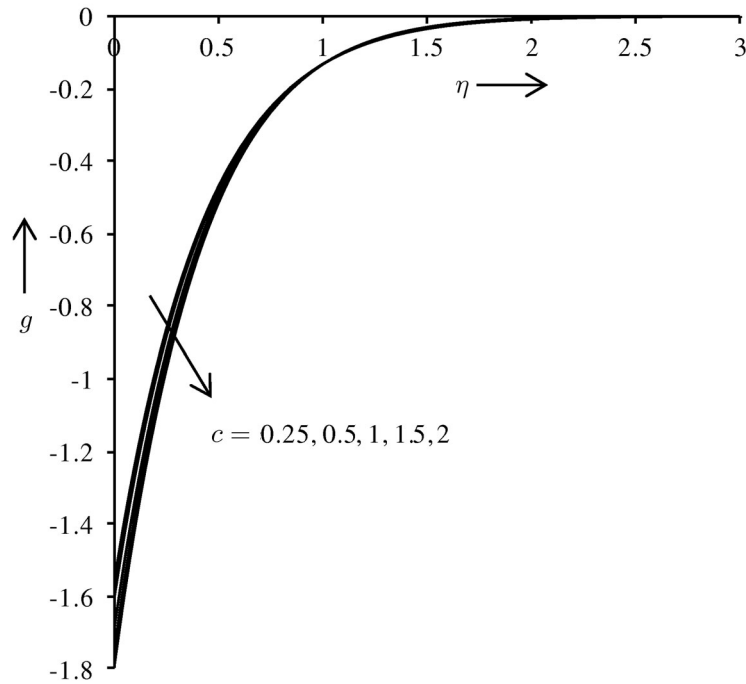
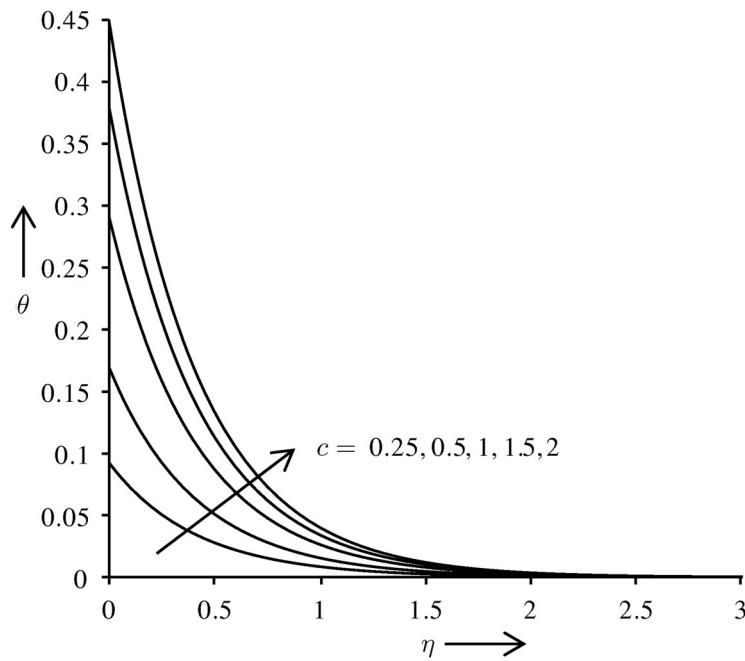**Fig. 6.** Microrotation distribution for different $c$ ($\lambda = 3.5$, $M = 3$, $n = 0.5$).



**Fig. 7.** Temperature distribution for different $c$ ($\lambda = 3.5$, $M = 3$, $n = 0.5$).

$c$ on the microrotation is depicted in Fig. 6. It is evident that as the convective parameter $c$ increases, microrotation decreases initially, but after covering a certain distance from the sheet all profiles converge and finally satisfy the far field boundary condition. Greater intensity in the convective boundary parameter is therefore observed to stifle gyratory motions of the micro-elements. This will serve to substantially alter the microstructure of the manufactured material. Figure 7 demonstrates that the temperature
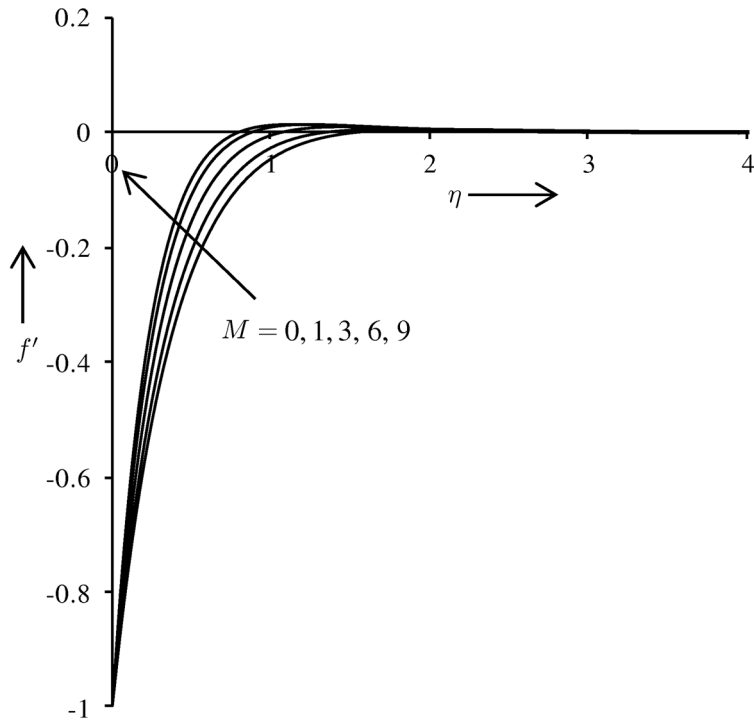
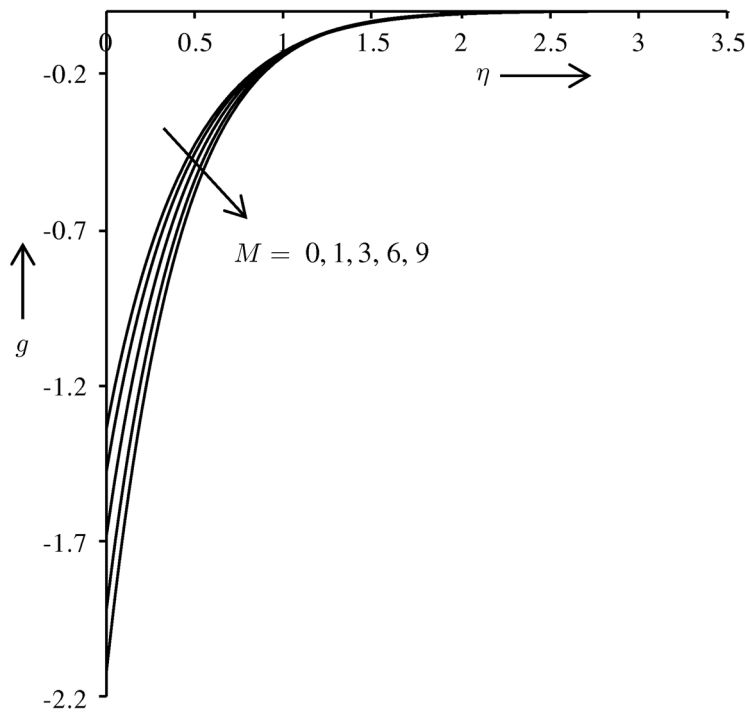**Fig. 8.** Velocity distribution for different $M$ ($\lambda = 3.5$, $c = 1$, $n = 0.5$).



**Fig. 9.** Microrotation distribution for different $M$ ($\lambda = 3.5$, $c = 1$, $n = 0.5$).

increases with elevation in convective parameter. It is also observed that the temperature attains a maximum at the surface and decreases gradually to the free stream temperature. Large values of $c$ result in lower thermal resistance of the sheet and higher convective heat transfer to the right side of the sheet. As a consequence of this, the heat transfer rate at the surface increases and this will exert a substantial effect on material characteristics. A similar observation has been reported by Aziz [33].
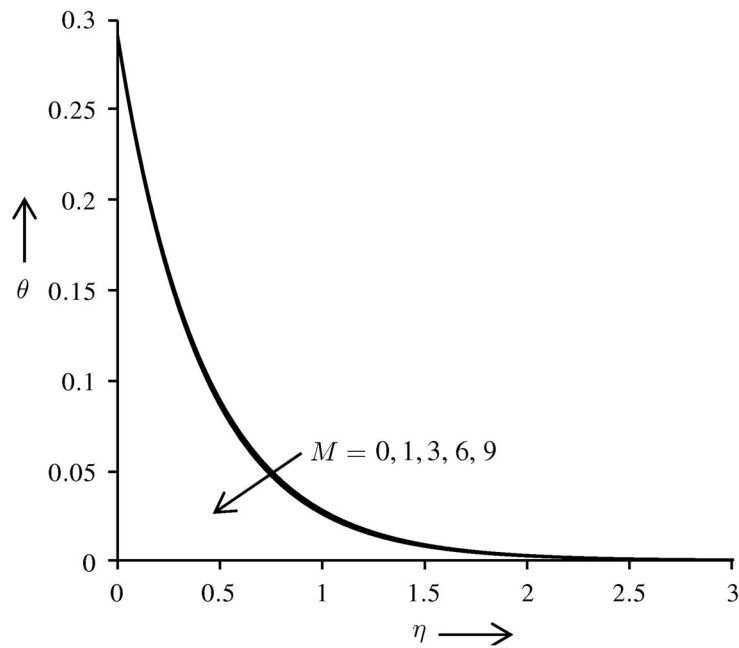
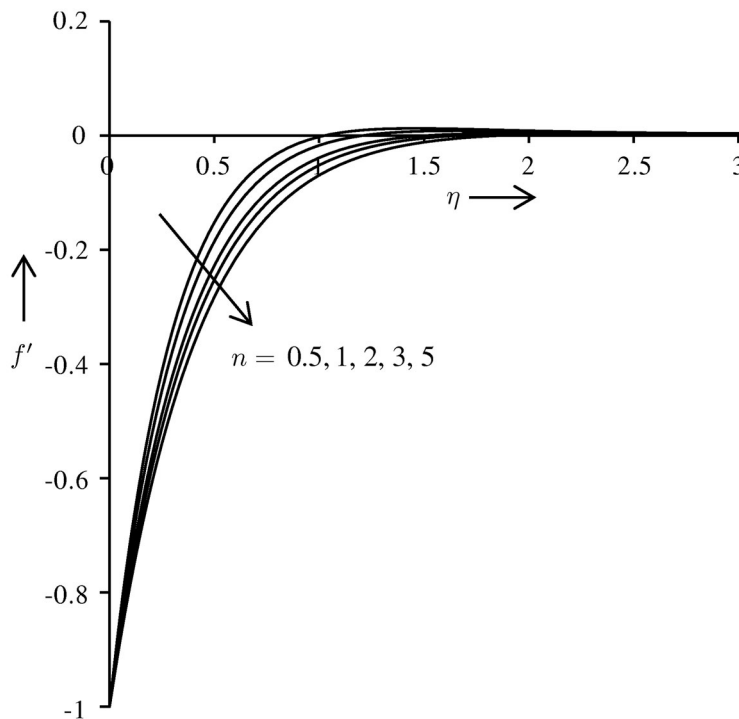**Fig. 10.** Temperature distribution for different $M$ ($\lambda = 3.5$, $c = 1$, $n = 0.5$).



**Fig. 11.** Velocity distribution for different $n$ ($\lambda = 3.5$, $c = 1$, $M = 3$).

From Fig. 8 some interesting observations can be made for velocity with the effect of magnetic parameter, $M$. Velocity magnitude decreases with an increase in the magnetic parameter, $M$. Accordingly, the boundary layer thickness decreases. In the presence of magnetic field a drag force called Lorentz force arises during the motion of electrically conducting fluid, which inhibits momentum development, i.e., retards the fluid. We note that the velocities generally have a negative value in Fig. 8, which is attributable more to the dominance of the shrinking sheet on the fluid physics. Figure 9 represents
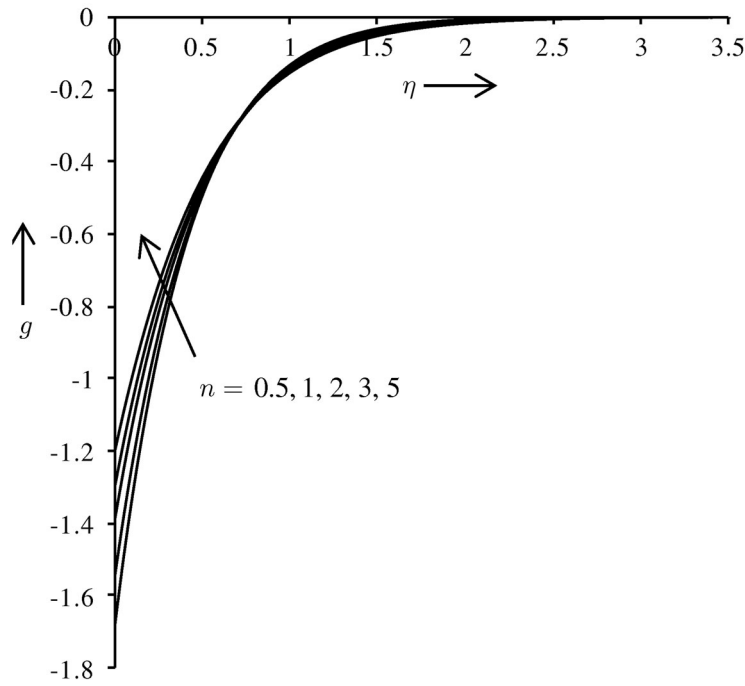
**Fig. 12.** Microrotation distribution for different $n$ ($\lambda = 3.5$, $c = 1$, $M = 3$).
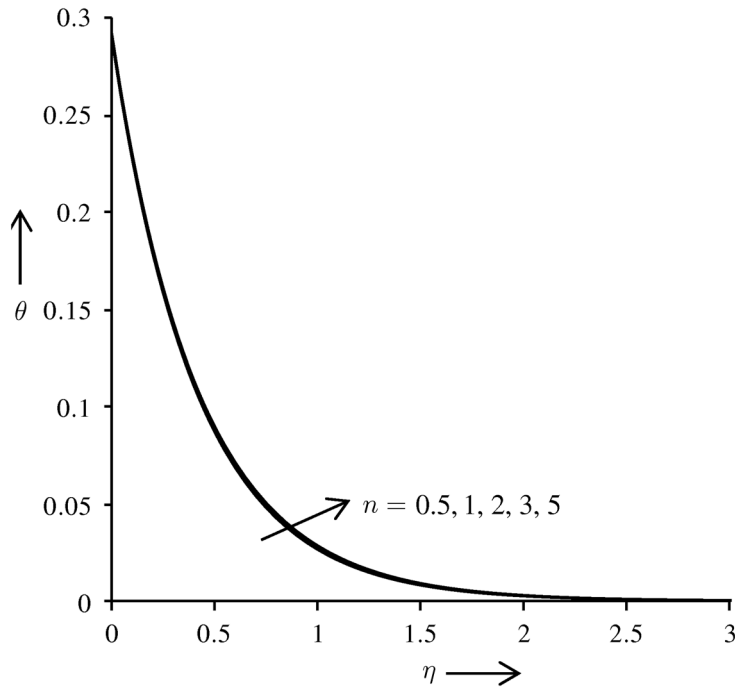


**Fig. 13.** Temperature distribution for different $n$ ($\lambda = 3.5$, $c = 1$, $M = 3$).

the microrotation distribution with the variation of the magnetic parameter $M$. It is noticed that the magnetic parameter $M$ causes a significant decrease in the microrotation for $0 \leq \eta < 1$, but for $\eta > 1$ all profiles merge indistinguishably and finally decay to zero. In all cases microrotation is negative, which shows the reverse rotation of microelements. Gyratory motions are therefore also inhibited with stronger magnetic field imposition. The impact of the magnetic parameter $M$ over the temperature distribution is shown in Fig. 10. Temperature of the fluid decreases slightly with increase in magnetic parameter. This is opposite to the effect generated in a stretching sheet flow, where temperature will be accentuated with

dissipation of thermal energy as a result of supplementary work done in dragging the magnetic field. Again the shrinking sheet physics has a major influence on the potency of magnetic field in the regime.

Figure 11 displays the variations of velocity within the boundary layer for different values of power index, $n$. As $n$ is enhanced, the shrinking sheet will contract faster. This will destroy momentum in the surrounding fluid and will cause a decrease in velocity, i.e., deceleration in the boundary layer flow, with increase in power index $n$. It is also noticed from the figure that velocity increases continuously from its initial value and approaches zero in the free stream, for any value of power-law index. Figure 12 depicts the effect of power index $n$ on the microrotation distribution. It is clear from the figure that microrotation increases initially with increase in $n$. For $\eta \approx 0.7$ all profiles intersect and thereafter microrotation decreases with increasing $n$. The effect of power index on the temperature is depicted in Fig. 13, from which we observe that no tangible influence in temperatures is caused with variation in $n$. This is understandable since $n$ is primarily a parameter influencing the momentum and angular momentum (mechanical variables) fields.

Table 3 demonstrates that skin friction (dimensionless surface shear stress function) decreases with increase in power index while it increases with an increase in suction, convective heat transfer and magnetic parameters. Thus the skin friction can be reduced effectively by introducing power index. It is evident from Table 4 that the rate of heat transfer increases with increase in suction parameter, convective heat transfer parameter, magnetic parameter, whereas decreases with increase in power index. It is also apparent that the rate of heat transfer is higher for larger values of convective heat transfer parameter. This is due to the fact that the left side of the sheet is heated by convection from hot fluid, and, therefore, the surface of the sheet becomes hotter and heat flows from the surface to the cool fluid on the right side. Thus effective cooling of the sheet can be achieved by implementing higher values of the convective heat transfer parameter. Generally the finite element solutions demonstrate good stability and convergence characteristics and the present code is being implemented to explore more complex geometries in the near future.

## 5. CONCLUSIONS

In the present paper we have investigated the influence of magnetic field on the steady mixed convection flow and heat transfer of an incompressible magneto-micropolar fluid over a nonlinear porous shrinking sheet. Using similarity transformations, the governing partial differential equations have been transformed into a set of nonlinear ordinary differential equations, which have been solved with an efficient, validated variational finite element method (FEM). It has been observed that the velocity and microrotation are affected significantly by suction parameter, convective heat transfer parameter, magnetic parameter, as well as with power index, whereas temperature is affected considerably by suction and convective heat transfer parameters. Numerical computations have shown that the drag can be reduced effectively with power index. It has also been noticed that at the surface the heat transfer rate is influenced more with a rise in the convective heat transfer parameter than all other parameters. Thus, the fast cooling of the surface can be achieved by the intelligent selection of the convective heat transfer parameter, which is desirable in industrial materials processing (e.g., electro-conductive polymers). The present study is restricted to the steady state flow and neglects the slip effects at the sheet. For future study, transient flow with slip effects at the sheet will be examined.

## NOTATIONS

$a$, $e$—constants
$B_0$—uniform magnetic field
$c$—convective heat transfer parameter
$c_p$—specific heat at constant pressure
$C_f$—skin friction coefficient
$f$—dimensionless velocity
$g$—dimensionless microrotation
$g_e$—gravitational acceleration
$h_f$—heat transfer coefficient
$Gr_x$—local Grashof number

$j$—microinertia density

$K$—coupling constant parameter

$M$—magnetic parameter

$n$—power index

$N$—microrotation component

$Nu_x$—local Nusselt number

$\mathrm{Pr}$—Prandtl number

$q$—heat flux

$\mathrm{Re}_x$—local Reynolds number

$S$—constant characteristic of the fluid

$T$—temperature of the fluid

$T_f$—temperature of the hot fluid

$T_w$—temperature of the surface

$T_\infty$—temperature of the ambient fluid

$u$—velocity in the $x$ direction

$U$—velocity of the sheet

$v$—velocity in the $y$ direction

$V_w$—velocity at the wall

$x$—distance along the surface

$y$—distance normal to the surface

*Greek Symbols*

$\beta$—coefficient of thermal expansion

$\gamma$—spin gradient viscosity

$\eta$—similarity variables

$\mu$—dynamic viscosity

$\rho$—density of the fluid

$\kappa$—thermal conductivity

$\nu$—kinematic viscosity

$\theta$—dimensionless temperature

$\sigma$—buoyancy parameter

$\sigma_0$—electrical conductivity

$\lambda$—suction parameter

$\phi$—stream function

$\tau_w$—wall shear stress

*Subscripts*

$w$—surface condition

$\infty$—conditions far away from the surface

# REFERENCES

1. Sakiadis, B.C., Boundary Layer Behavior on Continuous Solid Surfaces: Boundary-Layer Equations for Two-Dimensional and Axisymmetric Flow, *AIChemE J.*, 1961, vol. 7, pp. 26−28.
2. Tsou, F.K., Sparrow, E.M., and Goldstein, R.J., Flow and Heat Transfer in the Boundary Layer on a Continuous Moving Surface, *Int. J. Heat Mass Transfer*, 1967, vol. 10, pp. 219−235.
3. Crane, L.J., Flow past a Stretching Plate, *Z. Angew. Math. Phys.*, 1970, vol. 21, pp. 645−647.
4. Grubka, L.J. and Bobba, K.M., Heat Transfer Characteristics of a Continuous Stretching Surface with Variable Temperature, *ASME J. Heat Transfer*, 1985, vol. 107, pp. 248−250.
5. Elbashbeshy, E.M.A., Heat Transfer over a Stretching Surface with Variable Surface Heat Flux, *J. Phys. D: Appl. Phys.*, 1998, vol. 34, pp. 1951−1954.
6. Magyari, E. and Keller, B., Exact Solutions for Self-Similar Boundary-Layer Flows Induced by Permeable Stretching Walls, *Euro. J. Mechanics-B Fluids*, 2000, vol. 19, pp. 109−122.
7. Andersson, H.I., Slip Flow past a Stretching Surface, *Acta Mech.*, 2002, vol. 158, pp. 121−125.
8. Cortell, R., Effects of Viscous Dissipation and Radiation on the Thermal Boundary Layer over a Nonlinear Stretching Sheet, *Phys. Lett. A*, 2008, vol. 372, pp. 631−636.
9. Eringen, A.C., Theory of Micropolar Fluids, *J. Math. Mech.*, 1966, vol. 16, pp. 1−18.
10. Eringen, A.C., *Microcontinuum Field Theories II-Fluent Media*, 1st ed., New York: Springer, 2001.
11. Anwar Bég, O., Bhargava, R., and Rashidi, M.M., *Numerical Simulation in Micropolar Fluid Dynamics*, Germany: Lambert Academic Publishing, 2011.
12. Eringen, A.C., Theory of Thermomicrofluids, *J. Math. An. Appl.*, 1972, vol. 38, pp. 480−496.
13. Wang, C.Y., Liquid Film on an Unsteady Stretching Sheet, *Quart. Appl. Math.*, 1990, vol. 48, pp. 601−610.
14. Miklavcic, M. and Wang, C.Y., Viscous Flow Due to a Shrinking Sheet, *Quart. Appl. Math.*, 2006, vol. 64, pp. 283−290.
15. Goldstein, S., On Backward Boundary Layers and Flow in Converging Passages, *J. Fluid Mech.*, 1965, vol. 21, pp. 33−45.
16. Wang, C.Y., Stagnation Flow towards a Shrinking Sheet', *Int. J. Non-Linear Mech.*, 2008, vol. 43, pp. 377−382.
17. Bachok, N., Ishak, A., and Pop, I., Unsteady Three-Dimensional Boundary Layer Flow Due to a Permeable Shrinking Sheet, *Appl. Math. Mech.*, 2010, vol. 31, pp. 1421−1428.
18. Fang, T., Zhang, J., and Yao, S., Viscous Flow over an Unsteady Shrinking Sheet with Mass Transfer, *Chin. Phys. Lett.*, 2009, vol. 26, pp. 014703-4.
19. Fang, T., Yao, S., and Pop, I., Flow and Heat Transfer over a Generalized Stretching/Shrinking Wall Problem-Exact Solution of the Navier−Stokes Equations, *Int. J. Non-Linear Mech.*, 2011, vol. 46, pp. 1116−1127.
20. Bhattacharyya, K. and Layek, G.C., Effects of Suction/Blowing on Steady Boundary Layer Stagnation-Point Flow and Heat Transfer towards a Shrinking Sheet with Thermal Radiation, *Int. J. Heat Mass Transfer*, 2011, vol. 54, pp. 302−307.
21. Ishak, A., Lok, Y.Y., and Pop, I., Stagnation-Point Flow over a Shrinking Sheet in a Micropolar Fluid, *Chem. Eng. Comm.*, 2010, vol. 197, pp. 1417−1427.
22. Yacob, N.A. and Ishak, A., Micropolar Fluid Flow over a Shrinking Sheet, *Meccanica*, 2012, vol. 47, pp. 293−299.
23. Muhaimin, R. Kandasamy and A.B. Khamis, Effects of Heat and Mass Transfer on Nonlinear MHD Boundary Layer Flow over a Shrinking Sheet in the Presence of Suction, *Appl. Math. Mech.*, 2008, vol. 29, pp. 1309−1317.
24. Fang, T. and Zhang, J., Closed-Form Exact Solutions of MHD Viscous Flow over a Shrinking Sheet, *Comm. Nonlin. Sci. Numer. Simul.*, 2009, vol. 14, pp. 2853−2857.
25. Nadeem, S. and Hussain, A., MHD Flow of a Viscous Fluid on a Nonlinear Shrinking Sheet with Homotopy Analysis Method, *Appl. Math. Mech.*, 2009, vol. 30, pp. 1569−1578.
26. Schit, G.C. and Haldar, R., Effects of Thermal Radiation on MHD Viscous Flow and Heat Transfer over Nonlinear Shrinking Porous Sheet, *Appl. Math. Mech.*, 2011, vol. 32, pp. 677−688.
27. Hayat, T., Hussain, M., Hendi, A.A., and Nadeem, S., MHD Stagnation Point Flow towards Heated Shrinking Surface Subjected to Heat Generation/Absorption, *Appl. Math. Mech.*, 2012, vol. 33, pp. 631−648.
28. Ashraf, M. and Bashir, S., Numerical Simulation of MHD Stagnation Point Flow and Heat Transfer of a Micropolar Fluid towards a Heated Shrinking Sheet, *Int. J. Numer. Meth. Fluids*, 2012, vol. 69, pp. 384−398.
29. Das, K., Slip Effects on MHD Mixed Convection Stagnation Point Flow of a Micropolar Fluid towards a Shrinking Vertical Sheet, *Comp. Math. Appl.*, 2012, vol. 63, pp. 255−267.
30. Yilbas, B.S., Hussain, M.M., and Dincer, I., Heat and Moisture Diffusion in Slab Products Due to Convective Boundary Condition, *Heat Mass Transfer*, 2003, vol. 39, pp. 471−476.

31. Yilbas, B.S. and Kalyon, M., Analytical Solution for Pulsed Laser Heating Process: Convective Boundary Condition Case, *Int. J. Heat Mass Transfer*, 2002, vol. 45, pp. 1571–1582.
32. Wang, J., Wang, H., Sun, J., and Wang, J., Numerical Simulation of Control Ablation by Transpiration Cooling, *Heat Mass Transfer*, 2007, vol. 43, pp. 471–478.
33. Aziz, A., A Similarity Solution for Laminar Thermal Boundary Layer over a Flat Plate with a Convective Surface Boundary Condition, *Comm. Nonlin. Sci. Numer. Simul.*, 2009, vol. 14, pp. 1064–1068.
34. Ishak, A., Similarity Solutions for Flow and Heat Transfer over a Permeable Surface with Convective Boundary Condition, *Appl. Math. Comput.*, 2010, vol. 217, pp. 837–842.
35. Makinde, O.D. and Aziz, A., MHD Mixed Convection from a Vertical Plate Embedded in a Porous Medium with a Convective Boundary Condition, *Int. J. Therm. Sci.*, 2010, vol. 49, pp. 1813–1820.
36. Yao, S., Fang, T., and Zhong, Y., Heat Transfer of a Generalized Stretching/Shrinking Wall Problem with a Convective Boundary Conditions, *Comm. Nonlin. Sci. Numer. Simul.*, 2011, vol. 16, pp. 752–760.
37. Subhashini, S.V., Samuel, N., and Pop, I., Double-Diffusive Convection from a Permeable Vertical Surface under Convective Boundary Condition, *Int. Commun. Heat Mass Transfer*, 2011, vol. 38, pp. 1183–1188.
38. Makinde, O.D., Zimbab, K., and Anwar Bég, O., Numerical Study of Chemically-Reacting Hydromagnetic Boundary Layer Flow with Soret/Dufour Effects and a Convective Surface Boundary Condition, *Int. J. Therm. Environ. Eng.*, 2012, vol. 4, pp. 89–98.
39. Yacob, N.A. and Ishak, A., Stagnation Point Flow towards a Stretching/Shrinking Sheet in a Micropolar Fluid with a Convective Surface Boundary Condition, *Can. J. Chem. Eng.*, 2012, vol. 90, pp. 621–626.
40. Das, D., Sen, K., Saraogi, A., and Maity, S., Experimental Studies on Electro-Conductive Fabric Prepared by *In Situ* Polymerization of Thiophene onto Polyester, *J. Appl. Polymer Sci.*, 2010, vol. 116, pp. 3555–3561.
41. Bueschel, A., Klinkel, S., and Wagner, W., A Finite Element Formulation of a Viscoelastic Model for Dielectric Elastomers, *Proc. Appl. Math. Mech.*, 2011, vol. 11, pp. 359/360.
42. Chiam, T.C., Hydromagnetic Flow over a Surface Stretching with a Power-Law Velocity, *Int. J. Eng. Sci.*, 1995, vol. 33, pp. 429–435.
43. Reddy, J.N., *An Introduction to the Finite Element Method*, 3rd ed., New York: McGraw-Hill, 2005.
44. Gupta, D., Kumar, L., Anwar Bég, O., and Singh, B., Finite Element Simulation of Mixed Convection Flow of Micropolar Fluid over a Shrinking Sheet with Thermal Radiation, *Proc. IMechE, Part E: J. Proc. Mech. Eng.*, 2014, vol. 228, pp. 61–72.
45. Gupta, D., Kumar, L., and Singh, B., Finite Element Solution of Unsteady Mixed Convection Flow of Micropolar Fluid over a Porous Shrinking Sheet, *Sci. World J.*, 2014, article ID 362351.
46. Rana, P., Bhargava, R., and Anwar Bég, O., Numerical Solution for Mixed Convection Boundary Layer Flow of a Nanofluid along an Inclined Plate Embedded in a Porous Medium, *Comput. Math. Appl.*, 2012, vol. 64, pp. 2816–2832.
47. Kumar, L., Bhargava, R., Bhargava, P., and Takhar, H.S., Finite Element Solution of Mixed Convection Micropolar Fluid Flow between Two Vertical Plates with Varying Temperature, *Arch. Mech.*, 2005, vol. 57, pp. 251–264.
48. Anwar Bég, O., Curiel Sosa, J.L., and Liebana Murillo, J.M., Finite Element Analysis of Structural Instability Using a Switching Implicit–Explicit Technique, *Int. J. Comp. Meth. Eng. Sci. Mech.*, 2013, vol. 14, pp. 452–464.